Turbulence Lab Report, Group 6

Myriam Argaud, Lisa-Marie Eierding, Guillemette Flichy, Leona Kunzi, Romain Vincent

Abstract

The evolution of the turbulent flow is studied along the stream-wise axis in a wind tunnel downstream from an active grid, in order to investigate and understand the characteristics of an active grid-generated turbulence. The streamwise velocity was measured using hot-wire and Pitot-tube probes, and then the data were treated using Matlab. The turbulent kinetic energy decay, statistical properties, spatial scale and time scale are investigated. The results show that the flow verifies the turbulent energy cascade showing turbulent kinetic energy decay, and increase of integral length and time scale. The results also confirm that the flow after the active grid is homogeneous.

1. Introduction

Turbulence is a crucial phenomenon to study in fluid mechanics. Indeed, turbulence drives the behavior of flows in aerodynamics, climate dynamics, fluid distributions and more. For instance, the flow behind wind turbines and aerodynamic systems. Turbulent jets can be found behind aircraft engines, and turbulent skin friction drag accounts for the intensity of drag in transport systems. Homogeneous isotropic turbulence (HIT) is a type of turbulent flow worth investigating since it is used for theory development and concept understanding. It consists of fluctuating statistics that are independent of spatial position and coordinate system rotations and reflections.

Grid turbulence is an effective and straightforward way to create an approximation of HIT. The objective of this experiment is to investigate the stream-wise evolution of the grid-generated turbulence in regards to the characteristics of the flow and also to its decay in space.

The experiment measures the stream-wise velocity at several positions downstream of an active grid. The points are gradually spaced apart from the grid to acquire data on the flow's evolution.

The experiments were carried out using the active grid of the NTNU laboratory of fluid mechanics. More information about the effect of grid turbulence on the flow can be found in [1].

2. Theory

2.1. Homogeneous Isotropic Turbulence

Homogeneous isotropic turbulence (HIT) refers to a turbulent flow field in which the statistical properties are invariant concerning both position and direction. In such a flow, there is no mean flow. Homogeneous turbulence represents an idealized case that can be approximately realized in practice, for instance, in the nearly uniform turbulence downstream of a grid. Due to its relative simplicity, it is the most extensively studied form of turbulence [2].

The objective of this study is to generate an artificial approximation of homogeneous isotropic turbulence using an active grid. In the present work, the active grid is employed to induce random velocity fluctuations and thereby approximate the conditions of homogeneous and isotropic turbulence.

2.2. Turbulence Grids

Turbulence grids are used to create turbulence in the wind tunnel. There are two main types: passive and active grids. Both convert laminar flow in front of the grid into turbulent flow behind the grid.
An active grid is equipped with randomly moving elements designed to introduce velocity fluctuations into the flow, while passive grids are stationary structures. An important parameter regarding the grids is the mesh length M, which is going to be used in the subsequent sections of the report to refer to the distance behind the grid.

2.3. Turbulent Cascade

The fundamental mechanism of turbulence was described by Kolmogorov through the concept of the turbulent energy cascade in [3]. In this framework, energy is transferred from large-scale eddies — generated by large-scale perturbations — to progressively smaller scales. This cascade continues until the smallest dynamically relevant scale, known as the Kolmogorov scale η, is reached. The large-scale motion is typically characterized by the Reynolds number based on an integral length scale, $Re_L = \frac{UL}{\nu}$, where U and L denote characteristic velocity and length scales, respectively, and ν is the kinematic viscosity. At the Kolmogorov scale, the Reynolds number Re_η becomes

sufficiently small such that viscous dissipation dominates over inertial effects, leading to the conversion of kinetic energy into heat.
At sufficiently high Reynolds numbers, the energy balance described by the turbulent cascade needs to be fulfilled: the production of energy at the large scales is equal to the dissipation of energy at the small scales. This statement results in:

$$\varepsilon \sim \frac{\mathfrak{U}^3}{\mathfrak{L}}. \tag{1}$$

Under the assumption of HIT and u' being the characteristic velocity, one can rewrite Equation 1 as:

$$\varepsilon \sim \frac{k^{3/2}}{\mathfrak{L}}, \tag{2}$$

where $k = \frac{3}{2}\overline{u'^2}$. In this study, both the integral and Kolmogorov scales are employed to investigate the characteristics of the artificially generated turbulence.

2.4. Reynolds Decomposition

Reynolds decomposition is a common method that separates an instantaneous flow variable into the sum of two parts, a mean and a fluctuating component. This method is used in turbulence analysis to distinguish the steady trend from random velocity fluctuations. For the velocity field, it breaks the instantaneous velocity down into the mean velocity and the time-dependent velocity fluctuations $u(t) = U + u'(t)$.

2.5. Properties of Grid Turbulence

The grid-generated turbulence should have the following properties:

- homogeneous in the transverse plane:

$$U_2 \sim U_3 \sim 0$$
$$U_1 \neq 0$$
$$\frac{\partial \bar{\cdot}}{\partial x_2} = \frac{\partial \bar{\cdot}}{\partial x_3} = 0$$

- approximately isotropic:

$$\overline{u_1'} \sim \overline{u_2'} \sim \overline{u_3'}$$
$$1 \leq \frac{u_1'}{u_2'} \leq 1.2$$

- statistically stationary:

$$\frac{\partial \bar{\cdot}}{\partial t} = 0$$

- spatially decaying flow:

$$\frac{\partial k}{\partial x_1} \neq 0$$
$$\frac{\partial k}{\partial x_2} = \frac{\partial k}{\partial x_3} = 0$$

Assuming all these hypotheses are true, the turbulent kinetic energy equation

$$\frac{\partial k}{\partial t} + U_j \frac{\partial k}{\partial x_j} = -\overline{u_i' u_j'} \frac{\partial U_i}{\partial x_j} - \frac{1}{2} \frac{\partial \overline{u_i' u_i' u_j'}}{\partial x_j} - \frac{1}{\rho} \frac{\partial \overline{u_j' p'}}{\partial x_j} + \nu \frac{\partial^2 k}{\partial x_j^2} - \varepsilon \tag{3}$$

can be simplified to:

$$U_1 \frac{\partial k}{\partial x_1} = -\varepsilon \tag{4}$$

Then the turbulent kinetic energy follows a power law form in space, which is why Equation 4 can be written as:

$$\frac{k}{\overline{U_1'^2}} = A\left(\frac{x_1 - x_0}{M}\right)^{-n}. \tag{5}$$

The value of the exponent n is heavily discussed but expected to be close to 1.2 or 1.4 [4][5].

2.6. Taylor Frozen Hypothesis

To calculate the spatial gradient of the velocity, measurements must be done at several points of the stream. However, it could not be done without modifying the flow and disturbing the experiment. This is why the Taylor frozen hypothesis is used.

In the following experiment, it was considered that $u_1' \ll U_1$. Then:

$$\frac{\partial u_1'}{\partial x_1} = \frac{\partial t}{\partial x_1} \frac{\partial u_1'}{\partial t} = \frac{1}{u_1} \frac{\partial u_1'}{\partial t} \approx \frac{1}{U_1} \frac{\partial u_1'}{\partial t} \tag{6}$$

This hypothesis simplifies the experiment because the data can be taken at a given point at different times with a hot wire. The measurements are not disturbed by previous ones.

2.7. Statistical Tools

To analyze the flow, several statistical tools were used. The variance σ measures the width of the distribution.

$$\sigma = \overline{u_1'^2} \tag{7}$$

The skewness S characterized the symmetry of the statistical distribution. As the turbulence is supposed to be isotropic and homogeneous, the skewness should be near zero.

$$S = \frac{\overline{u_1'^3}}{\overline{u_1'^2}^{\frac{3}{2}}} \tag{8}$$

The kurtosis K measures the frequency of extreme events. In other words, it characterizes the distribution disparity.

$$K = \frac{\overline{u_1'^4}}{\overline{u_1'^2}^2} \tag{9}$$

2.8. Relevant Quantities

The Dissipation ε and the dissipation constant C_ε are calculated using the Taylor frozen flow hypothesis. For homogeneous, isotropic turbulence, the formula for the dissipation is the following

$$\varepsilon = 15\nu\overline{\left(\frac{\partial u_1'}{\partial x}\right)^2}. \tag{10}$$

For intermediate scales Equation 10 can be rewritten as

$$\varepsilon = 15\nu\left(\frac{\overline{u_1'^2}}{\lambda^2}\right). \tag{11}$$

The dissipation constant, a dimensionless representation of the rate of turbulent energy dissipation in a flow, is calculated through

$$C_\varepsilon = \frac{\varepsilon L_{11}}{\overline{u'}^{3/2}}.$$

The in 2.3 mentioned Kolmogorov microscale η is calculated by

$$\eta = \frac{\nu^{3/4}}{\varepsilon^{1/4}}. \tag{12}$$

The Taylor microscale λ provides a statistical measure of the intermediate scales within a flow. It typically marks the point where viscous effects become significant, serving as a boundary between inertial-dominated scales and those influenced primarily by viscosity and energy dissipation. It is determined by

$$\lambda^2 = \frac{\overline{u_1'^2}}{\overline{\partial u_1'/\partial x_1}^2}. \tag{13}$$

The Taylor Reynolds number Re_λ uses the Taylor microscale as the characteristic length scale. It is typically used to identify how turbulent a flow is. The calculation is performed as

$$Re_\lambda = \frac{\sqrt{\overline{u_1'^2}}\lambda}{\nu} = \frac{u_1'\lambda}{\nu}. \tag{14}$$

The integral length scale L_{11} quantifies the characteristic size of the largest energy-containing eddies within the flow. It is obtained by

$$L_{11} = \frac{1}{\overline{u_1'^2}}\int_0^\infty \overline{u_1'(x_1)\,u_1'(x_1+r)}\,dr. \tag{15}$$

In the following sections, the evolution of the flow generated by the active grid is studied. The HIT hypotheses are verified. The decay exponent for the turbulent kinetic energy k is investigated.

3. Method

The experiments were carried out in a closed-loop wind tunnel in the fluid mechanics laboratory at NTNU. The wind tunnel has a working section that is 2.71 m wide, 1.8 m high and 11 m long. A schematic representation of the experimental setup is provided in Figure 1. The quasi-laminar flow in the wind tunnel passed through an active turbulence grid, with flow characteristics determined by airflow settings and grid rotation parameters. To investigate the downstream decay of turbulent kinetic energy behind the grid, the velocity fluctuations were measured using a hot-wire probe. The probe was mounted on a translational measurement system that progressively moved downstream away from the grid, taking measurement points spaced according to the predetermined sampling time. The probe measures the heat flux away from the wire due to turbulence and provides a voltage signal in time. Conversion of this signal to velocity data necessitated calibration using a Pitot-static tube, which provided reference measurements of mean flow velocity.

3.1. Wind Tunnel and Active Grid

The experiment was conducted using an active grid with a mesh length of $M = 0.1$ m, used to create turbulence evolving through time and much more homogeneous than with a passive grid. The active grid consists of 90 shafts to which agitator wings of size 0.1 m are attached. The active grid was operated with randomized rotational velocities following a top-hat distribution. For this experiment, the frequencies and sampling time chosen are $\Omega = 3 \pm 1.5$ Hz and $t_s = 240$ s. The frequency range of the active grid was chosen close to the one used in previous experiments done on grid turbulence and found in [1]. The sampling time was chosen to ensure a sufficiently large dataset for subsequent data analysis.

According to [6], the experiment should be set as a zero pressure gradient $\frac{\partial p}{\partial x_1} = 0$. This is why the tunnel roof is not perfectly parallel to the floor but slopes up to open up the test section and, therefore, counterbalance the pressure deficit due to the increasing boundary layer thickness.

3.2. Pre-Calibration

Two probes were mounted on the mobile measurement system. A calibration protocol was established to determine the relationship between the hot-wire anemometer voltage output and the corresponding flow velocity. The hot-wire signals were recorded using a data acquisition (DAQ) system and correlated with simultaneous measurements obtained from a Pitot-static tube. Additionally, the initial atmospheric pressure was measured using a mercury barometer and incorporated into the data acquisition script. The initial temperature was also measured to compare it with the final temperature, giving the temperature change $\Delta T = T_{final} - T_{initial}$.

A total of eleven calibration points were collected. For each point, the flow velocity was varied by adjusting the rotational speed of the ventilator to span the entire velocity range required for the pre-calibration. At each calibration point, velocity measurements were obtained using both a Pitot-static tube and a hot-wire anemometer. During the entire calibration procedure, the active grid remained inactive to ensure undisturbed flow conditions.

3.3. Streamwise Scans

A series of 13 data points was acquired. At each point, the values were measured for 4 min and afterwards, the measuring system was moved downstream to the next point. The downstream positions were taken from $25M$ to $80M$ behind the grid. The freestream velocity in the test section was maintained at a constant value of $U_1 = 8.4\,\mathrm{m\,s^{-1}}$. The data from the hot wire, Pitot tube, pressure and ambient temperature was collected by the students and operated through the Matlab script that had been provided.

Moreover, a temperature correction was employed in the processing script to prevent perturbations from any change of temperature, following the temperature correction method presented in [7].

3.4. Post-Calibration

Once all data points have been covered, post-calibration was performed to account for potential sensor drift issues. The atmospheric pressure was measured again using a mercury barometer and entered into the Matlab script. The procedure is the same as for the pre-calibration.

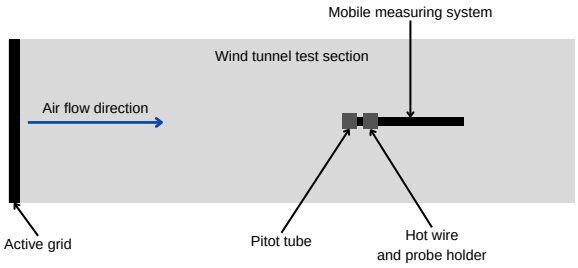

Figure 1: Experimental setup in the wind tunnel

4. Results

4.1. Pre- and Post-Calibration

In Figure 2, one can see the measured and normalized mean velocity during pre- and post-calibration over the measured and normalized voltage. The x-axis is compensated by the temperature change ΔT. It can be seen that the shift between the measured values is minor. Only for the highest flow velocity can a small deviation be observed.

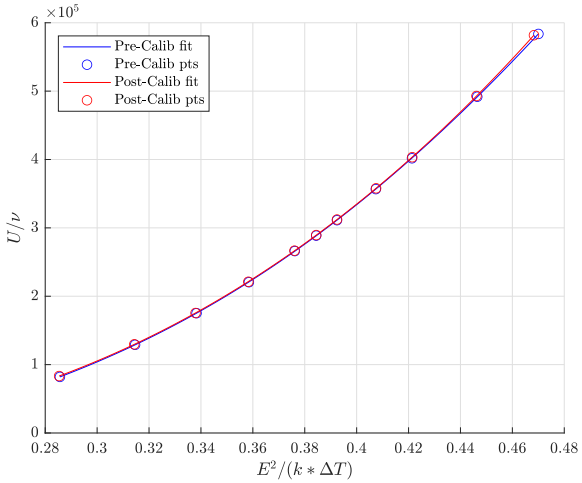

Figure 2: Normalised voltage and velocity measurement during pre- and post-calibration

4.2. Statistical Convergence

The turbulent velocity measured is a random signal over time. It thus requires a sampling time long enough to capture a sufficient number of samples of the velocity and thus ensure an accurate estimate of the velocity statistics. To confirm the validity of the experiment's sampling time, convergence plots were calculated for the mean velocity U_1 and the fluctuations u_1' at three downstream positions: $25M$, $52M$ and $80M$. There are two plots for each measurement point.

The analysis presented in Figure 3 is based on assessing the convergence of the mean and the variance of the streamwise velocity component as a function of sampling duration. Therefore, the statistics are evaluated after certain time steps t_i, shown on the x-axis of the plots. For each sampling duration t_i, multiple non-overlapping subsamples with the same length t_i were extracted from the full velocity time series. The total number of sub-samples is approximately $\frac{t_i}{t_s}$, where t_s denotes the total duration of the original time series.

One figure shows the relative error in the mean velocity, evaluated for each sub-sample. This is calculated as

$$\varepsilon_{mean} = \frac{U_1 - U_{1,f}}{U_{1,f}} \tag{16}$$

where U_1 is the mean velocity over the entire dataset, and $U_{1,f}$ the mean velocity within a sub-sample of duration t_i. This metric (or "error") quantifies the deviation of subsample means from the global mean, thereby illustrating how the statistical convergence of the mean improves with increasing sampling duration.

The second figure presents a similar analysis for the variance of the fluctuating velocity component u_1'. The

plotted quantity is

$$\varepsilon_{var} = \frac{\overline{u_1'^2} - \overline{u_{1,f}'^2}}{\overline{u_{1,f}'^2}} \tag{17}$$

where u_1' is the variance over the full signal, and $u_{1,f}'$ is the variance computed over a sub-sample of length t_i. This relative error indicates how accurately the sub-sample captures the total turbulent kinetic energy in the streamwise direction. A decrease in the scatter of this quantity with increasing t_i supports the adequacy of the total sampling time t_s for converged turbulence statistics.

4.3. Turbulence Statistics

For each data point, kurtosis and skewness were calculated and plotted over the distance from the grid (see Figure 4). Additionally, the probability density function (PDF) was plotted for the first and last data point (25 and 80 mesh length), which can be seen in Figure 5.

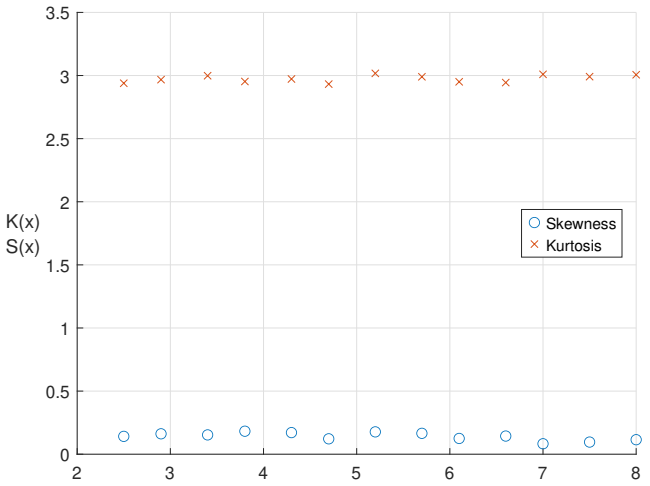

Figure 4: Evolution of the skewness and kurtosis along the data points

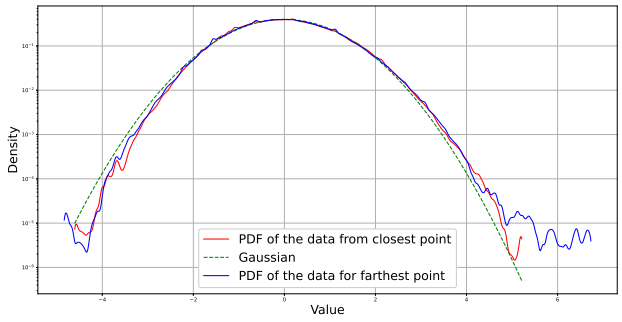

Figure 5: Probability density function plotted in semi-log scale for $25M$ and $80M$, and a Gaussian distribution with the same standard deviation as the velocity distributions superimposed

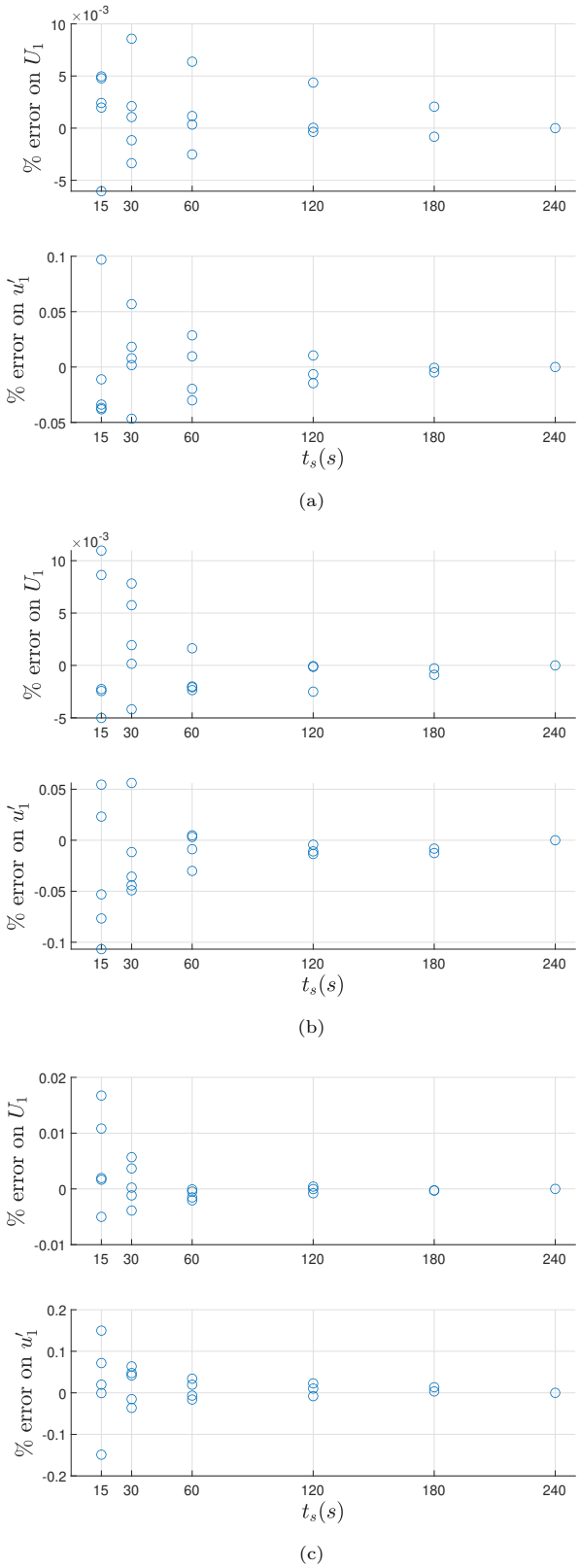

Figure 3: (a) Convergence of U_1 and u_1' at $25M$ from the grid (b) Idem at $52M$ (c) Idem at $80M$

4.4. Turbulence Spectrum and Turbulent Kinetic Energy Decay

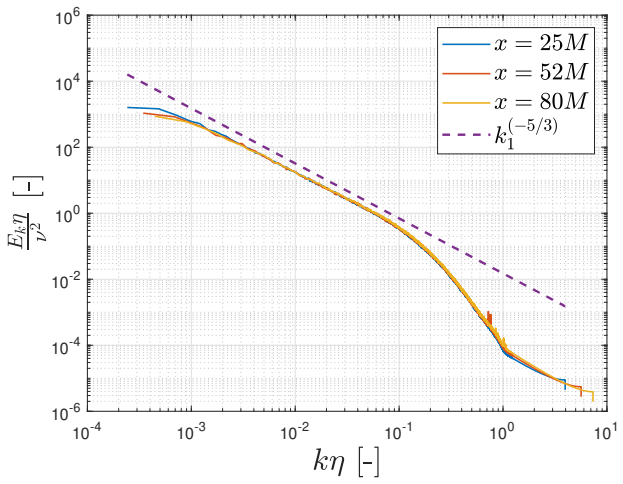

Figure 6: Turbulence Spectrum at $25M$, $52M$ and $80M$

Figure 6 shows the power spectra of the stream-wise velocity fluctuations at three downstream positions ($25M$, $52M$, and $80M$), plotted against the normalized wavenumber $k\eta$.

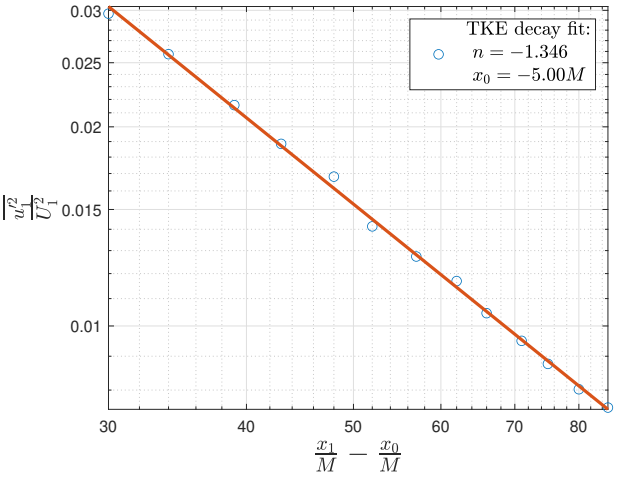

Figure 7: TKE Decay over Distance

Figure 7 presents the normalized turbulent kinetic energy $\overline{u_1'^2}/U_1^2$ as a function of streamwise position $\frac{x_1 - x_0}{M}$ on a log-log scale. The decay value of the exponent n was calculated using a fitting algorithm [8].

4.5. Integral Length and Time Scale

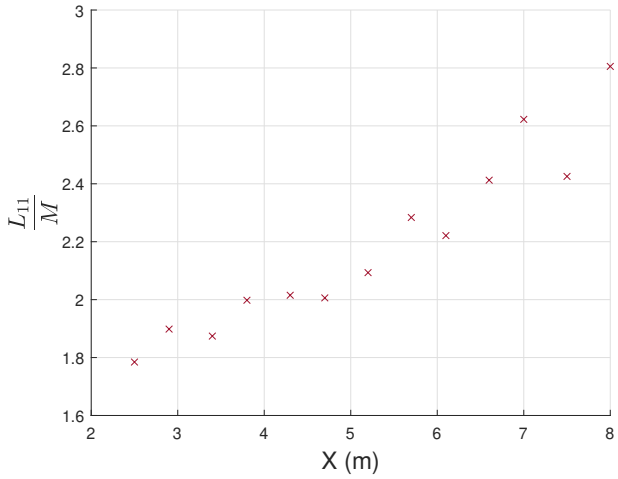

Figure 8: Spatial Evolution of the Integral Length Scale

Figure 8 illustrates the evolution of the integral time and length scales. Overall, both quantities increase with the downstream position, as the dashed lines indicate. The similarity in their evolution is expected, given their linear correlation according to Taylor's frozen hypothesis.

4.6. Dissipation

The dissipation decreases over the distance from the active grid. The drop mentioned above is graphically illustrated in Figure 9. On the other hand, the dissipation constant is increasing in space as seen in Figure 10.

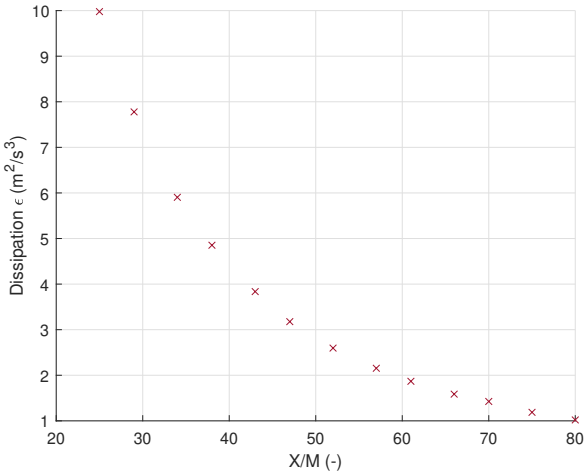

Figure 9: Spatial evolution of the dissipation

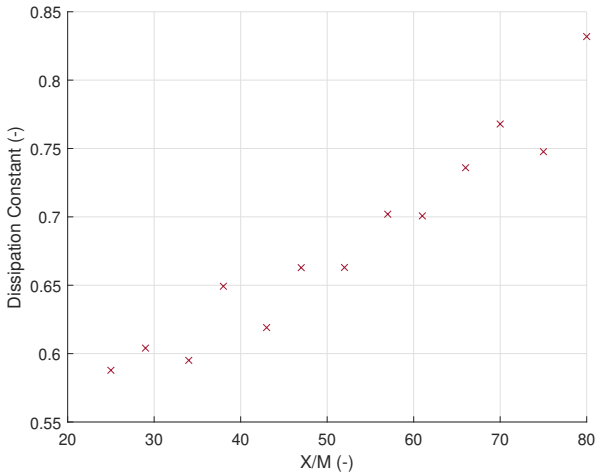

Figure 10: Spatial evolution of the dissipation constant

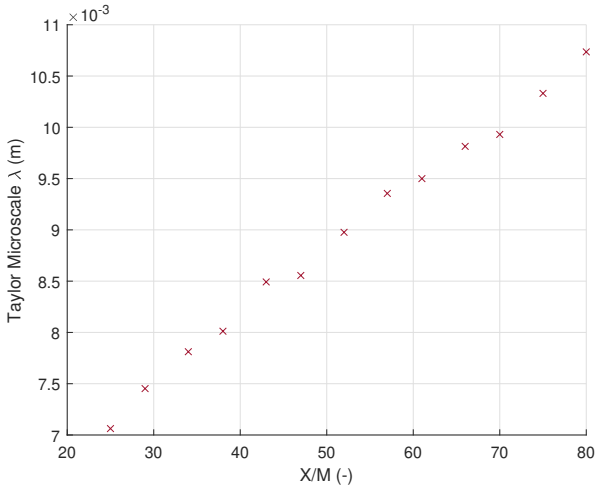

Figure 12: Spatial evolution of the Taylor Microscale

4.7. Length Scales

The spatial evolution of the different length scales in the flow was investigated. As can be seen in Figure 11, the Kolmogorov Microscale increases linearly with distance from the active grid.

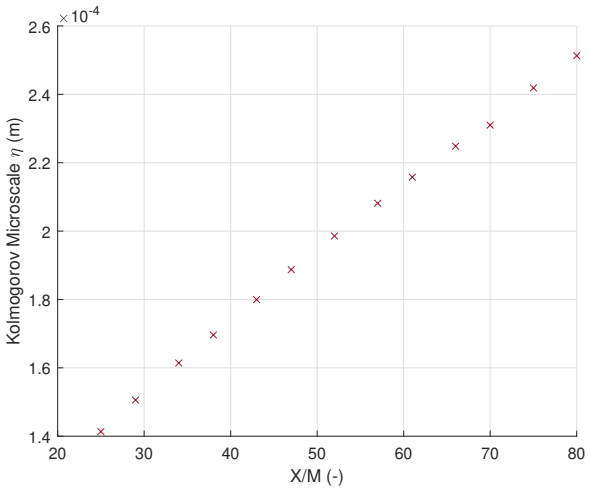

Figure 11: Spatial dvolution of the Kolmogorov Microscale

The Taylor Microscale is also increasing with the distance from the grid as seen in Figure 12. The Taylor Reynolds Number, on the other hand, decreases in space, which is represented in Figure 13.

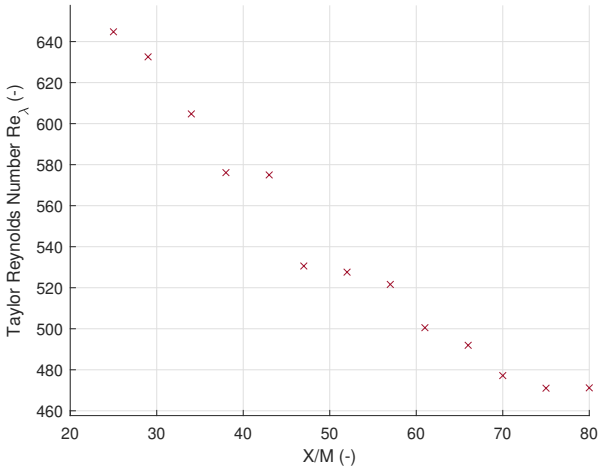

Figure 13: Spatial evolution of the Taylor Reynolds Number

5. Discussion

5.1. Pre- and Post-calibration

The voltage measurements from the hot-wire anemometer were calibrated against the corresponding flow velocities measured by the Pitot-static tube. A fifth-order polynomial fit was applied to the calibration data. The resulting calibration curves before and after the measurement campaign exhibit a high degree of similarity, indicating that no significant sensor drift occurred. A slight deviation was observed at the highest velocity; however, given the small magnitude of this discrepancy and the consistency of the remaining data points, the shift is considered negligible.

5.2. Statistical Convergence

The six plots, provided in Figure 3, show that the average speeds, calculated over shorter times, are randomly

distributed around the total average value. This means that the average value stayed consistent over the entire measurement time.

The plots also show that the scatter in the data reduces as the sampling time is increased. This indicates that the total sampling time t_s enabled statistical convergence to be reached. The sampling time used was thus long enough to ensure an accurate estimate of the velocity statistics.

5.3. Turbulence Statistics

An active grid is used to generate a homogeneous and quasi-isotropic turbulence. To investigate the homogeneity of the turbulence after the grid, the PDF, skewness, and kurtosis of the closest and farthest points to the grid are interpreted. It is not possible to investigate the isotropy of the turbulence since all of the available data is in the streamwise direction.

In the first place, Figure 5 shows that the two probability density functions are similarly close, and they show good agreement with the Gaussian distribution. The PDFs at the other data points were also plotted and appeared similar but are not presented here. This contributes to confirming the homogeneity of the flow. Indeed, the deviations from the Gaussian distribution are limited and are due to the evolution in time of the fluctuations. This agreement is characteristic of developed, homogeneous and isotropic turbulence.

Secondly, kurtosis and skewness remain stable across the data points, as can be seen in Figure 4. This also confirms the similarity of the evolution of the velocity fluctuations across the points, and thus the homogeneity of the turbulence. The values of skewness are almost zero, which indicates an almost symmetric distribution, meaning balanced acceleration and deceleration events, and the kurtosis is almost three. These values are characteristic of a Gaussian distribution and thus homogeneous turbulence.

The investigation of statistical tools that are available in this experiment are all consistent in indicating that the test section of the wind tunnel has indeed homogeneous turbulence, as required by the HIT hypothesis made in the theory section.

5.4. Turbulence Spectrum and Turbulent Kinetic Energy Decay

The temporal and spatial evolution of turbulence is fundamentally governed by the energy cascade and the progressive dissipation of kinetic energy. The present experiment is designed to capture these mechanisms using an analysis of turbulent kinetic energy decay and the spectral distribution of velocity fluctuations.

5.4.1. Turbulence Spectrum

All three curves in Figure 6 exhibit an inertial subrange, indicated by the dashed purple line, where the spectral slope approaches the classical Kolmogorov scaling of $-\frac{5}{3}$. This confirms the persistence of the energy cascade mechanism, wherein energy is transferred from large-scale eddies to smaller scales before being dissipated by viscosity.

As the distance from the turbulence-generating grid increases, the spectra gradually shift downward, reflecting the overall decay in energy.

Also, while the spectral peaks slightly shift and decrease with x, their overall shape remains consistent, pointing to a stable energy distribution across scales despite spatial decay.

5.4.2. TKE Decay

The linear trend observed in Figure 7 confirms that the decay follows a power-law behavior, consistent with the classical theory of turbulence in homogeneous isotropic turbulence. This behavior aligns with the theoretical expression:

$$\frac{\overline{u_1'^2}}{U_1^2} = A\left(\frac{x_1 - x_0}{M}\right)^{-n}$$

The slope of this line can be directly linked to the decay exponent n, which here is equal to $n = -1.346$. This value for the decay exponent belongs to the range of the experimental values commonly reported in literature, which range between $n = -1.2$ and $n = -1.5$ for decaying homogeneous isotropic turbulence.

The good agreement between the measured data and the fitted power law further validates the assumption of a power-law decay regime in this flow configuration. The placement of the virtual origin upstream of the first measurement point also aligns with classical turbulence decay models, suggesting that the turbulence started developing before the measurement domain.

5.5. Integral Length Scale and Time Scale

With increasing downstream distance, the integral length scale L_{11} exhibits a growth trend, indicating that large eddies expand as they move away from the grid. This behavior is expected as smaller eddies progressively merge into larger structures, leading to an overall increase in their characteristic size. The further downstream the flow develops, the more pronounced this merging effect becomes. Notably, a peak in L_{11} and T is observed at $X = 7\,\mathrm{m}$, which may be attributed to measurement noise or systematic errors in the data acquisition process.

Similarly, the integral time scale increases with downstream distance, implying that larger eddies persist for longer durations. According to Taylor's frozen flow hypothesis, the integral time scale and integral length scale are linearly related by a factor of $1/\overline{U_i}$. Consequently, their evolution follows a similar trend.

5.6. Dissipation

In Figure 7, it can be observed that the turbulent kinetic energy decreases in space as there is no external energy input. The power law 2 shows the link between k and the dissipation ε. A decrease in k therefore leads directly to a decrease in dissipation as stated in Equation 2.
The dissipation constant is a measure of how strong the energy is dissipated through viscous effects. As the decrease of the dissipation is smaller than the increase of L_{11} and the decrease of $\overline{u'}$, the dissipation constant increases. The relation is shown in Equation 2.8. This means that the efficiency of the energy transfer is increased in a relative sense.

5.7. Length Scales

The decrease of the dissipation ϵ results in an increase of the Kolmogorov Microscale η as can be seen in Equation 12. This means that the small-scale structure of the turbulence becomes coarser. This is consistent with the general smoothing of the flow.

The Taylor Microscale λ is dependent of k and ε (see Equation 11). As ε decreases in space, λ has to increase. As already mentioned, the Taylor Reynolds number is directly dependent on λ and, therefore, shows the same behavior.
In conclusion, this means that the smaller eddies die down first so that only the large eddies remain in the end.

6. Conclusion

An active grid in a wind tunnel was successfully used to generate an approximate HIT flow. The turbulent energy cascade was highlighted as well as the decay of turbulent kinetic energy. The statistics of the generated turbulence were discussed, as well as different time and length scales. They were found to be consistent with the properties of the HIT. The accuracy of the results was assured by studying the statistical convergence, mean velocity and fluctuations. In conclusion, the results validate the effectiveness of the active grid in reproducing key features of homogeneous isotropic turbulence.

References

[1] R. J. H. Oddbjørn Kildal, Leon Li, et al., On the use of an active turbulence grid in wind tunnel testing of bridge decks, Journal of Wind Engineering Industrial Aerodynamics 233 (105331) (2023).

[2] W. D. Stewart Glegg, Aeroacoustic of low mach number flow (2017).

[3] A. N. Kolmogorov, A refinement of previous hypotheses concerning the local structure of turbulence in a viscous incompressible fluid at high reynolds number, Journal of Fluid Mechanics 13 (1) (1962).

[4] D. D. A. Panickacheril John John, S. K. R., Laws of turbulence decay from direct numerical simulations, Phil. Trans. R. Soc. A. (2022).

[5] L. Li, Turbulent flows lecture notes, Norges teknisk-naturvitenskapelige universitet courses (TEP4112) (2025).

[6] S. C. Geneviève Comte Bellot, The use of a contraction to improve the isotropy of grid-generated turbulence, Journal of fluid mechanics, The Johns Hopkins University 25 (1965).

[7] A. J. S. Marcus Hultmark, Temperature corrections for constant temperature and constant current hot-wire anemometers (2010).

[8] R. J. Hearst, P. Lavoie, Decay of turbulence generated by a square-fractal-element grid, Journal of Fluid Mechanics (2014) Page 576.